JACS
JOURNAL OF THE AMERICAN CHEMICAL SOCIETY
Communication
pubs.acs.org/JACS

Real-Time Imaging of the Formation of Au–Ag Core–Shell Nanoparticles

Shu Fen Tan,[†,⊗] See Wee Chee,[‡,§,∥,⊥,⊗] Guanhua Lin,[‡,§,∥,⊥] Michel Bosman,[#,▽] Ming Lin,[#] Utkur Mirsaidov,[*,‡,§,∥,⊥] and Christian A. Nijhuis[*,†,⊥]

[†]Department of Chemistry, National University of Singapore, 3 Science Drive 3, Singapore 117543

[‡]Centre for Bioimaging Sciences and Department of Biological Sciences, National University of Singapore, 14 Science Drive 4, Singapore 117543

[§]Department of Physics, National University of Singapore, 2 Science Drive 3, Singapore, 117551

[∥]NUSNNI-Nanocore, National University of Singapore, 5A Engineering Drive 1, Singapore, 117411

[⊥]Centre for Advanced 2D Materials and Graphene Research Centre, National University of Singapore, 6 Science Drive 2, Singapore 117546

[#]Institute of Materials Research and Engineering, A*STAR (Agency for Science, Technology and Research), 2 Fusionopolis Way, Singapore 138634

[▽]Department of Materials Science and Engineering, National University of Singapore, 9 Engineering Drive 1, Singapore 117575

Supporting Information

ABSTRACT: We study the overgrowth process of silver-on-gold nanocubes in dilute, aqueous silver nitrate solution in the presence of a reducing agent, ascorbic acid, using *in situ* liquid-cell electron microscopy. Au–Ag core–shell nanostructures were formed via two mechanistic pathways: (1) nuclei coalescence, where the Ag nanoparticles absorbed onto the Au nanocubes, and (2) monomer attachment, where the Ag atoms epitaxially deposited onto the Au nanocubes. Both pathways lead to the same Au–Ag core–shell nanostructures. Analysis of the Ag deposition rate reveals the growth modes of this process and shows that this reaction is chemically mediated by the reducing agent.

Core–shell nanoparticles are highly functionalized nanoparticles (NPs) with distinctive properties that originate from controlled chemical composition, morphology, and surface properties. The functionality of the core–shell NPs can, for example, be altered by changing the core-to-shell volume ratio.[1] This tunability allows for the control of the NP's properties for many applications, ranging from controlled drug delivery,[2,3] catalysis,[4,5] and electronic band structure control[6] to photoluminescence enhancement.[7,8]

The synthesis of core–shell NPs with different morphologies and compositions can be accomplished by various chemical means, such as solution-phase reduction,[9,10] and physical methods, such as wire electrical explosion followed by ultrasonic irradiation.[11] Fine-tuning of the surface structure, i.e., the dominant crystalline facets, and surface composition is important for catalytic applications, and can be accomplished with the addition of chemical additives during the synthesis. For instance, addition of poly(vinylpyrrolidone) to the reaction mixture in the synthesis of Au–Ag core–shell NPs results in {111} facets,[12] while addition of *N,N*-dimethylformamide and ethylene glycol (EG) gives similar NPs but with {100} facets.[13] In general, the experimental conditions that control NP growth are identified empirically, and the NP morphology is confirmed with the so-called "quench-and-look" approach, where the reaction is stopped at various stages, after which the intermediate reaction products are imaged with microscopic techniques such as transmission electron microscopy (TEM). However, early stages of the reactions, short-lived intermediate structures, and the dynamics of the reactions cannot be investigated in this way. As such, how the chemical additives, such as capping agents and reducing agents, play a part in controlling the composition and morphology of the NP still remains largely unresolved. Clarifying these questions is important, as it will help us to understand how processes such as deposition and surface diffusion of shell atoms are affected by these additives during the evolution of a core seed into core–shell nanocrystal with a well-defined shape and composition.

In the case of chemically synthesized Au–Ag cubic core–shell NPs, the focus of this work, Lim et al.[14] reported that the Au cubes nucleate and grow homogeneously along the six low-index (100) planes of the cubic seeds when a strong reducing agent, L-ascorbic acid (AA, or Vitamin C), is used. They attributed this observation to fast reducing kinetics by AA, which promote the formation of {100} facets in the presence of bromide ions from the capping agent, cetyltrimethylammonium bromide (CTAB). Others proposed that the overgrowth is promoted by the presence of the Br^- ions[9,10,15] and that the size of the shell depends on the ratio of precursor and reducing agent and the size of the core.[9,13,14,16,17] The capping agent plays a crucial role in stabilizing high-energy facets and, hence, in the resulting shape of the nanostructure. After all, if high-energy facets are not stabilized, the thermodynamically most

Received: January 17, 2016
Published: April 4, 2016

DOI: 10.1021/jacs.6b00594
J. Am. Chem. Soc. 2016, 138, 5190–5193

stable shape will be obtained. It is still not clear how the deposition of the shell takes place and whether the shell grows via a single pathway or a combination of pathways. Recently, *in situ* techniques have been more commonly applied to address such questions.[18−20]

In situ liquid-cell (LC) electron microscopy is an emerging technique for elucidating the mechanisms of the formation of nanostructures in real time with nanometer-scale resolution.[18−20] It is also well known that the electron beam itself can act as a reducing agent that reduces metal ions through the action of solvated electrons from radiolysis of water. This effect has been exploited to investigate the nucleation of Ag NPs directly from aqueous Ag precursor solutions.[21,22] Recently, Jungjohann et al.[16] and Wu et al.[17] demonstrated the use of *in situ* LC microscopy to study the solution growth of Au−Pd and Pt−Au core−shell NPs, respectively.

Here, we use LC-TEM to investigate the formation of Au−Ag core−shell nanocubes in real time. The Au seeds were prepared beforehand by following a method described by Sun et al.[23] and then washed to remove the capping agent (see Supporting Information (SI) for details). This washing procedure was necessary because we found that imaging of the nanocubes and their reaction dynamics was obscured when the stock solution with 20.0 mM CTAB was used, due to micelle formation. The reaction dynamics could only be clearly seen through the liquid below the critical micelle concentration of 1.0 mM.[24,25] Hence, we washed away the excess CTAB to ensure we could follow the Au−Ag core−shell NP formation well. We also showed that 0.1 and 1.0 mM concentrations of CTAB did not change the outcome of the Ag shell formation (see SI, section 7). Next, the Au seeds were drop-casted on the SiN_x window of the liquid cell, followed by assembly of the liquid cell, and the liquid cell was mounted on the TEM holder. The Ag precursor solution was introduced via flow tubing after the holder was loaded into the TEM. The experiments were carried out at room temperature. The NPs were continuously imaged from the start of liquid flow; the time $t = 0$ in any of the movies is defined when we first observed a change in a nanocube morphology (see SI, page S2 for details).

Figure 1 shows typical structures that were formed when Ag precursor solution was introduced to Au nanocubes in the absence of AA (using the electron beam as reducing agent). We did not observe formation of the Au−Ag core−shell nanostructures under electron beam irradiation (see SI, movie 1). Instead, the electron beam reduced the Ag^+ ions in solution, which then nucleated into Ag nanoclusters. These Ag clusters attached to the Au nanocubes randomly (red arrows), growing in a non-conformal manner, resulting in irregular structures.

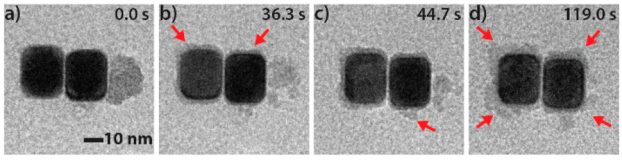

Figure 1. Time-lapse TEM images showing two Au nanocubes (black) interacting with the Ag precursor solution in the absence of L-ascorbic acid inside a liquid flow cell. NPs are coated with Ag (gray) shell. Red arrows indicate Ag shell formation on the Au nanocubes.

In subsequent experiments, we reverted to the conventional recipe by premixing the Au nanocubes with AA before introducing the Ag precursor solution into the mixture. Figure 2a−e shows time-lapsed TEM images of the Au−Ag nanostructures that were observed *in situ*. In this case, the Ag shell is conformal and homogeneous instead of randomly attached Ag clusters (Figure 1). Moreover, these core−shell nanostructures are similar in terms of morphology to those prepared *ex situ* (Figure 2f). Both preparations yield NPs with {110} facets (Figure 2a) and similar shell thicknesses of 7 ± 3 nm (Figure 2g,h). Hence, we propose that while the electron beam can reduce silver nitrate, it does not induce the overgrowth reaction after premixing.

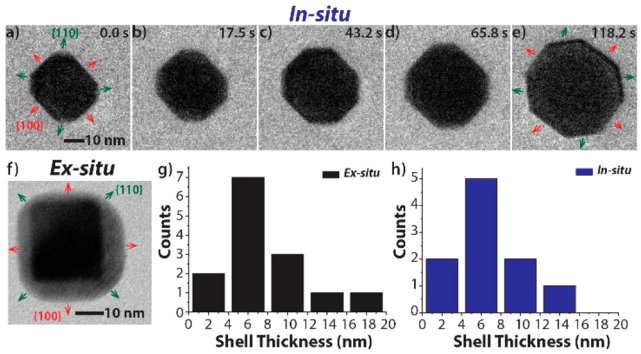

Figure 2. (a−e) Time-lapse TEM images showing a Au nanocube interacting with the Ag precursor solution in the presence of L-ascorbic acid (AA) inside a flow cell. (f) TEM image of *ex situ*-prepared Au−Ag core−shell nanostructures with addition of AA. (g,h) Histograms of Ag shell thicknesses for Au−Ag core−shell NPs that were prepared by (g) *ex situ* and (h) *in situ* (at time point where the nanostructures stopped growing) methods.

These results contradict the overgrowth model proposed previously[9,10,14,15] where the Br^- ions were crucial in the formation of homogeneous Ag shells. The Au nanocubes used in our experiments were washed and little residual CTAB was left in solution. The lack of available CTAB is also evidenced by the Au nanocubes gradually transforming into cubes with rounded corners with time after washing (see SI, Figure S7). We also performed control experiments at different concentrations of CTAB (see SI, section 7) and with a different capping agent, CTAC (see SI, section 8). In both cases, the shell formation was observed. Therefore, our results show that shells around a nanocube only form in the presence of AA regardless the concentration and type of capping agent used. From these observations, we conclude that AA plays a previously unknown, but important role in guiding the overgrowth of Ag on Au in the early stages of the reaction.

An advantage of *in situ* microscopy is that we can directly observe the dynamics of the growth of the shell. Two pathways for the overgrowth process were reported earlier, either by adatom deposition or by the attachment of preformed clusters from solution.[26] We found that both growth pathways occur in parallel in our experiments. Figure 3 shows two time series of TEM images where a single Au nanocube reacts with the Ag precursor solution inside a liquid flow cell. Figure 3a shows a Au nanocube that grows a homogeneous layer of Ag through monomer attachment (see SI, Movie 2). In contrast to the image sequence in Figure 3c, no Ag NPs are observed throughout the whole growth process. Moreover, the Ag shell thicknesses d at the edge (d_E) and corner (d_C) as a function of the reaction time t increase steadily as a function of time without sudden jumps (Figure 3e).

DOI: 10.1021/jacs.6b00594
J. Am. Chem. Soc. 2016, 138, 5190−5193

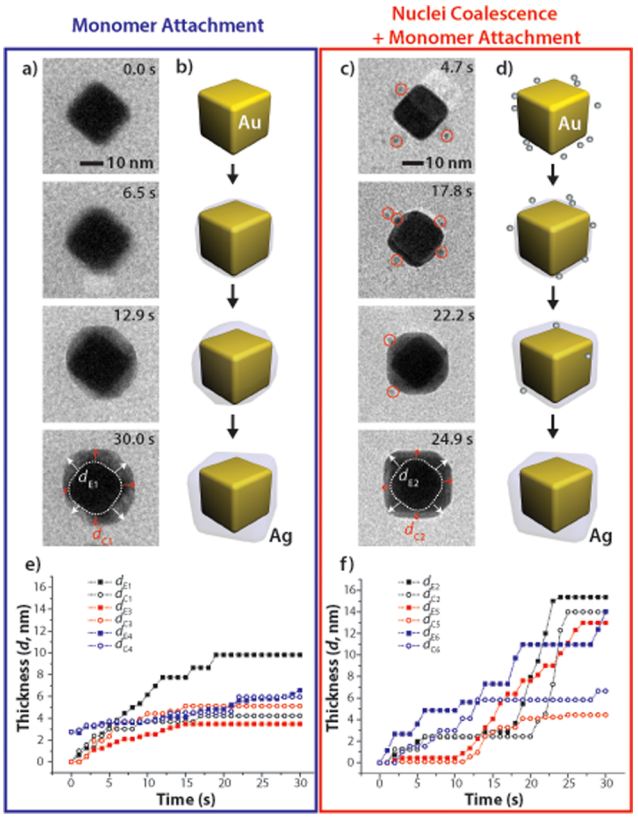

Figure 3. Time-lapse TEM images of a Au nanocube interacting with the Ag precursor solution inside a flow cell via (a) monomer attachment process and (c) monomer attachment and nuclei coalescence. (b,d) Schematics of the reaction between Au nanocubes and Ag nitrate aqueous solution for the two pathways. (e,f) Measured thicknesses of the edge (d_E, solid squares) and corner (d_C, hollow circles) of the Au–Ag core–shell particle as a function of time for the two pathways. The measurement of edge and corner thicknesses is done over six real-time movies of six different particles (three particles for each pathway). Note: d_{E1} and d_{C1} refer to measured thicknesses of edge and corner as denoted by white arrows and red arrows, respectively, in panel (a); $d_{E3,4}$ and $d_{C3,4}$ refer to other real-time movies with the same pathway, while d_{E2} and d_{C2} refer to measured thicknesses of edge and corner as denoted by white arrows and red arrows, respectively, in panel (b); $d_{E5,6}$ and $d_{C5,6}$ refer to other real-time movies with the same pathway. The white shadows in panels (a) and (c) are scattering artifacts.

Figure 3c shows Ag NPs that formed in the solution approach and attach onto the Au nanocubes and then form a homogeneous layer of Ag via coalescence, resulting in a well-defined Au–Ag NP (see SI, Movie 3). The small Ag NPs with a diameter of ~3 nm (encircled in red) are clearly visible at t = 4.7 s. We propose that these small Ag NPs are formed either when the silver nitrate solution is brought in contact with the AA solution inside the liquid cell or through radiolysis, i.e., reduction of the Ag^+ ions by solvated electrons as shown in Figure 1. The image recorded at t = 17.8 s and the subsequent images show that the small Ag NPs attach onto the surface of the Au nanocube and then coalesce (Figure 3c: t = 22.2 s) into a continuous layer (Figure 3c: t = 24.9 s). In addition, the increase of the Ag shell thickness d at the edge (d_E) and corner (d_C) as a function of the reaction time t is nonlinear (Figure 3f). Particularly, the shell thickness increases drastically from t = 19.2 s to t = 24.9 s, while the Ag NPs disappear. There is no lag time between Ag NPs attachment and the sudden increase in d which implies that the Ag NPs are absorbed into the Ag layer, resulting in the sudden jump in shell thickness. Both pathways lead to the same final product, i.e., Au–Ag core–shell NPs with similar values for the shell thickness. For both pathways, the shell growth stops after some time, regardless of the amount of Ag precursor solution flown into the liquid cell. The termination of Ag layer growth does not appear to be the result of local precursor depletion. We observed Ag NPs formation at the periphery of the electron beam, on the viewing screen outside the field of view of the CCD camera, which indicates that fresh solution is being continuously introduced into the cell.

Earlier studies showed that the shape of the final product is strongly dependent on the ratio between the deposition rate and the surface diffusion.[27] When the rate of surface diffusion is faster than the atom deposition rate, the reaction is driven by thermodynamics, where the adatoms diffuse and migrate to the site that is the lowest in surface free energy; therefore, the growth of the shell will be along ⟨100⟩ and ⟨110⟩ directions (Figure 3a,c). Depending on the presence of a capping agent such as CTAB to suppress growth at the higher surface energy faces, it is possible to tune the reaction outcome to form either a cuboctahedron (capping agent poor, Figure 4a) or a truncated

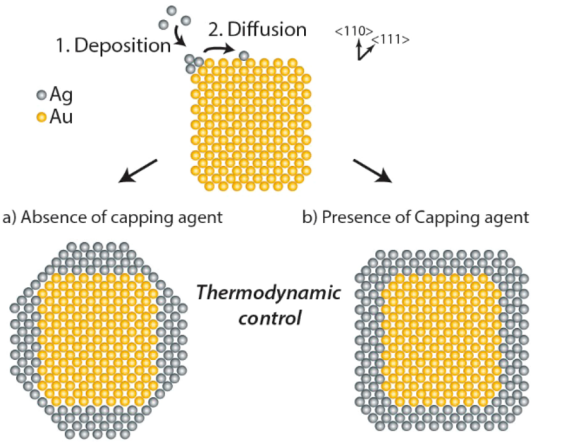

Figure 4. Schematic illustrations showing the shape evolution of a cubic seed under thermodynamic control for two conditions: (a) absence or (b) presence of capping agents. This model is adapted from Xia et al.[27]

cube (capping agent rich, Figure 4b). This process is referred to as thermodynamic control.[27] On the other hand, if the atom deposition rate is higher than the surface diffusion rate, the shell growth mode may switch to one that promotes the formation of more complex shapes, such as a concave cube or an octapod, due to preferential attachment to certain faces. Such reactions are considered to be under kinetic control.

Therefore, the development of {110} facets in both *in situ* and *ex situ* results (see SI, Figure S6) indicates that the growth mechanism is thermodynamically controlled with the absence or low coverage of capping agents. Furthermore, the *in situ* results also indicate that atomic deposition is not the only mechanism by which the Ag layer grows. The coalescence and integration of Ag NPs (that formed in solution) into a growing shell implies that the growth can also take place via a nonclassical growth mechanism where crystals grow via attachment, reorientation, and coalescence of smaller nanocrystals.[28,29]

DOI: 10.1021/jacs.6b00594
J. Am. Chem. Soc. 2016, 138, 5190–5193

We present an *in situ* study of the overgrowth process of Ag onto Au nanocubes in the presence of a reducing agent (AA) and with low capping agent concentration (CTAB) by *in situ* TEM microscopy. Our results show that the initial overgrowth is chemically mediated by AA and not by CTAB. We also observe two different mechanistic pathways that coexist for the formation of the Ag shell: (1) Ag NPs formed in solution deposit onto the Au nanocube as a result of coalescence, and (2) Ag adsorbs directly on Au via monomer attachment. Both mechanistic pathways lead to the same final product, i.e., Au−Ag NPs with the same Ag thickness and morphology. Silver coverage is absent when only the electron beam was used to reduce the Ag precursor, and comparison with *ex situ* synthesized nanostructures suggests that the observed growth reaction is insensitive to the electron beam and that AA plays a controlling role in the Au−Ag NP formation. In this case, the final morphology of the core−shell structure is that of a cuboctahedron, due to insufficient availability of CTAB in the solution. This study shows that not only can we study growth mechanisms with *in situ* LC-TEM, but the technique can also be used to elucidate the role of the chemical additives. Future work could address the possibility of altering the reaction kinetics by screening different kinds of chemical additives, which would be useful for materials engineering in nanofabrication.

■ ASSOCIATED CONTENT

Supporting Information

The Supporting Information is available free of charge on the ACS Publications website at DOI: 10.1021/jacs.6b00594.

Experimental details and materials characterization (PDF)

Real-time movie 1, showing typical structures formed when Ag precursor solution was introduced to Au nanocubes in the absence of AA, using electron beam as reducing agent AVI)

Real-time movie 2, showing growth of a homogeneous layer of Ag on a Au nanocube through monomer attachment (AVI)

Real-time movie 3, showing formation of Ag NPs in the solution that approach and attach onto the Au nanocubes and then form a homogeneous layer of Ag via coalescence (AVI)

Movie 4, a reconstructed 3D view showing a rounded Ag shell coating on the Au nanocube (MPG)

■ AUTHOR INFORMATION

Corresponding Authors

*phyumm@nus.edu.sg

*christian.nijhuis@nus.edu.sg

Author Contributions

⊗S.F.T. and S.W.C. contributed equally to this work

Notes

The authors declare no competing financial interest.

■ ACKNOWLEDGMENTS

The National Research Foundation (NRF) is kindly acknowledged for supporting this research under the CRP programs (award nos. NRF-CRP 8-2011-07 and NRFCRP9-2011-04).

■ REFERENCES

(1) Oldenburg, S. J.; Averitt, R. D.; Westcott, S. L.; Halas, N. J. *Chem. Phys. Lett.* **1998**, *288*, 243.

(2) Laurent, S.; Forge, D.; Port, M.; Roch, A.; Robic, C.; Vander Elst, L.; Muller, R. N. *Chem. Rev.* **2008**, *108*, 2064.

(3) Dresco, P. A.; Zaitsev, V. S.; Gambino, R. J.; Chu, B. *Langmuir* **1999**, *15*, 1945.

(4) Daniel, M.-C.; Astruc, D. *Chem. Rev.* **2004**, *104*, 293.

(5) Gawande, M. B.; Goswami, A.; Asefa, T.; Guo, H.; Biradar, A. V.; Peng, D.-L.; Zboril, R.; Varma, R. S. *Chem. Soc. Rev.* **2015**, *44*, 7540.

(6) Kortan, A. R.; Hull, R.; Opila, R. L.; Bawendi, M. G.; Steigerwald, M. L.; Carroll, P. J.; Brus, L. E. *J. Am. Chem. Soc.* **1990**, *112*, 1327.

(7) Mews, A.; Eychmueller, A.; Giersig, M.; Schooss, D.; Weller, H. *J. Phys. Chem.* **1994**, *98*, 934.

(8) Ma, G. H.; He, J.; Rajiv, K.; Tang, S. H.; Yang, Y.; Nogami, M. *Appl. Phys. Lett.* **2004**, *84*, 4684.

(9) Ma, Y.; Li, W.; Cho, E. C.; Li, Z.; Yu, T.; Zeng, J.; Xie, Z.; Xia, Y. *ACS Nano* **2010**, *4*, 6725.

(10) Gong, J.; Zhou, F.; Li, Z.; Tang, Z. *Langmuir* **2012**, *28*, 8959.

(11) Fu, W.; Yang, H.; Chang, L.; Li, M.; Bala, H.; Yu, Q.; Zou, G. *Colloids Surf., A* **2005**, *262*, 71.

(12) Qi, X.; Balankura, T.; Zhou, Y.; Fichthorn, K. A. *Nano Lett.* **2015**, *15*, 7711.

(13) Tsuji, M.; Matsuo, R.; Jiang, P.; Miyamae, N.; Ueyama, D.; Nishio, M.; Hikino, S.; Kumagae, H.; Kamarudin, K. S. N.; Tang, X.-L. *Cryst. Growth Des.* **2008**, *8*, 2528.

(14) Lim, B.; Kobayashi, H.; Yu, T.; Wang, J.; Kim, M. J.; Li, Z.-Y.; Rycenga, M.; Xia, Y. *J. Am. Chem. Soc.* **2010**, *132*, 2506.

(15) Cho, E. C.; Camargo, P. H. C.; Xia, Y. *Adv. Mater.* **2010**, *22*, 744.

(16) Jungjohann, K. L.; Bliznakov, S.; Sutter, P. W.; Stach, E. A.; Sutter, E. A. *Nano Lett.* **2013**, *13*, 2964.

(17) Wu, J.; Gao, W.; Wen, J.; Miller, D. J.; Lu, P.; Zuo, J.-M.; Yang, H. *Nano Lett.* **2015**, *15*, 2711.

(18) Mirsaidov, U. M.; Zheng, H.; Bhattacharya, D.; Casana, Y.; Matsudaira, P. *Proc. Natl. Acad. Sci. U. S. A.* **2012**, *109*, 7187.

(19) Zheng, H.; Smith, R. K.; Jun, Y.-w.; Kisielowski, C.; Dahmen, U.; Alivisatos, A. P. *Science* **2009**, *324*, 1309.

(20) Liao, H.-G.; Niu, K.; Zheng, H. *Chem. Commun.* **2013**, *49*, 11720.

(21) Woehl, T. J.; Evans, J. E.; Arslan, I.; Ristenpart, W. D.; Browning, N. D. *ACS Nano* **2012**, *6*, 8599.

(22) Noh, K. W.; Liu, Y.; Sun, L.; Dillon, S. J. *Ultramicroscopy* **2012**, *116*, 34.

(23) Sun, J.; Guan, M.; Shang, T.; Gao, C.; Xu, Z.; Zhu, J. *Cryst. Growth Des.* **2008**, *8*, 906.

(24) Ruiz, C. C. *Mol. Phys.* **1995**, *86*, 535.

(25) Aguiar, J.; Carpena, P.; Molina-Bolívar, J. A.; Carnero Ruiz, C. *J. Colloid Interface Sci.* **2003**, *258*, 116.

(26) Smeets, P. J. M.; Cho, K. R.; Kempen, R. G. E.; Sommerdijk, N. A. J. M.; De Yoreo, J. J. *Nat. Mater.* **2015**, *14*, 394.

(27) Xia, Y.; Xia, X.; Peng, H.-C. *J. Am. Chem. Soc.* **2015**, *137*, 7947.

(28) Penn, R. L.; Soltis, J. A. *CrystEngComm* **2014**, *16*, 1409.

(29) Ataee-Esfahani, H.; Skrabalak, S. E. *RSC Adv.* **2015**, *5*, 47718.

DOI: 10.1021/jacs.6b00594
J. Am. Chem. Soc. 2016, 138, 5190−5193